Detection of defects in a 2D fluid-solid periodic cluster

Hamza Hafidi Alaoui, Samuel Rodriguez, Marc Deschamps

Detection of defects in a 2D fluid-solid periodic cluster

Hamza Hafidi Alaoui[a], Samuel Rodriguez[a,1], Marc Deschamps[b]

[a] *University of Bordeaux, CNRS, Arts et Metiers Institute of Technology, Bordeaux INP, INRAE, I2M Bordeaux, F-33400 Talence, France*
[b] *CNRS, University of Bordeaux, Arts et Metiers Institute of Technology, Bordeaux INP, INRAE, I2M Bordeaux, F-33400 Talence, France*

Abstract

The present work deals with locating a defect buried in a medium composed of a fluid matrix and small solid inhomogeneities. Classical imaging methods are based on delay and sum principle and would implicitly assume that the undamaged medium is homogeneous. The topological imaging framework however allows to take into account the heterogeneous nature of the undamaged medium and potentially to take advantage of it. In this work, it is applied to a demanding test case with different assumptions on the knowledge of the medium properties using a specifically-designed fluid-solid compatible imaging function. It leads to the definition of three imaging processes whose results are compared using respectively synthetic and experimental data. The results show the relevance of using the inhomogeneities' locations information, but not necessarily at all steps of the imaging process, leading to the definition of so called hybrid topological imaging method.
Keywords: Nondestructive Testing; Ultrasonic Waves; Topological Imaging; Heterogeneous Medium; Multiple scattering; Periodic Cluster.

Bullet Points

- Topological imaging allows locating a defect buried in a periodic cluster.
- Topological imaging takes advantage of medium heterogeneity to enhance resolution.
- An imaging function adapted to fluid-solid heterogeneous media is proposed.
- Classical imaging methods are retrieved from the topological imaging framework.

Email addresses: hamzaalaouihafidi@gmail.com (Hamza Hafidi Alaoui), samuel.rodriguez@u-bordeaux.fr (Samuel Rodriguez), marc.deschamps@u-bordeaux.fr (Marc Deschamps)
[1] Corresponding author

1. Introduction

The detection, localization, and monitoring of the evolution of defects in diffusive media have received a lot of attention because of the underneath theoretical interest and the large number of industrial applications. Wave propagation in such media is complex and the challenge is that the signature of the defect is hidden in the acoustic field reflected by the structure itself independently of the defect. In the present work, only active ultrasonic inspection is considered. The principle of active inspection is summarized in the following steps: one or several source(s) emit(s) a wave into the medium; it is scattered by the inhomogeneities and the resulting wave is measured by the same or other sensor(s). The measurement contains single scattering and multiple scattering contributions. Several methods have been implemented to process the information contained in the backscattered waves in order to characterize or image the medium. In a globally homogeneous one-polarisation non-dispersive isotropic infinite or semi-infinite medium, the presence of a single or a few inhomogeneities modify the wave field in a manner that multiple scattering contribution is small in comparison to single scattering. In this case, we consider that the incident wave undergoes only one scattering event before propagating to the sensor(s). This is the contribution used in conventional imaging techniques, that rely on the direct relation between the arrival time t of the echo and the distance d between the sensors and the scatterers, $t = 2d/c$ (c is the sound velocity). These analytical models of propagation allow the definition of efficient imaging methods based on the delay and sum principle such as Synthetic Aperture Focusing Technique [1] and Total Focusing method [2]. In more complex media, these methods require some improvements. Dispersion can be compensated for [3] whereas anisotropy requires more complex processing [4]. In the presence of several simultaneous wave polarizations, an experimental 2D sampling of the medium allows discriminating them [5]. This step is required as each polarization corresponds to a different wave velocity.

In reverberating or diffusive media, the conventional imaging methods based on the delay and sum principle fail to detect or to locate the defects because the single scattering assumption is not valid as multiple scattering contribution is dominant. In random heterogeneous media, like concrete for instance, the waves are scattered multiple times by heterogeneities. The challenge in inspecting such media is to deal with all the effects of the different objects in the wave propagation model. The issue of characterization and imaging of random or even heterogeneous media has received special

attention in the three past decades. The methods developed for this purpose can be classified into two distinct categories: imaging methods without the prior knowledge of the local properties of the heterogeneous medium, and others that use a partial or complete scattering model obtained from the local properties of the medium. The methods presented in the present work belong to the second category. Short reviews of both categories are respectively given in the next subsections.

1.1. Imaging methods for unknown heterogeneous media

The diffusion model is one of the most used models to describe the wave propagation phenomena in unknown heterogeneous media because the energy of the waves is transported in a way which is similar to the diffusion of heat. G. Bal and O. Pinaud [6] use the macroscopic model of the diffusion equation to detect an inclusion buried in highly heterogeneous random media. The imaging of the medium is based on the analysis of the fluctuations of the diffusion coefficient (estimated from energy measurements) caused by the buried inclusions. The method is illustrated by numerical simulations in two-dimensional space. Most of the results presented in this article have been generalized to other macroscopic models such as the radiative transfer equation [7]. However, this approach needs heavy numerical computations. Moreover, the final resolution of the image is limited by the transport mean free path of the scattering medium instead of half the wavelength. A. Aubry and A. Derode present another method to solve the same problem. Using a transducer array, the impulse responses between all array elements are measured and form a matrix. A filtration operation is then applied to this matrix in order to separate the single scattering contribution of the inclusion from the multiple scattering contribution. The detection of the target is achieved applying the DORT method [8] (french acronym for the decomposition of the time reversal operator) to the filtered matrix. Finally, the random matrix theory is used to give a detection criterion. This method is successfully applied to detect and image defects in highly scattering experimental media [9], and weakly scattering media [10]. It is shown that the quality of detection is significantly better than what is obtained with classical imaging methods, but this technique is limited to the detection of a strong scatterer and is not sensitive to weak perturbations. In many practical applications such as monitoring volcanoes and bioacoustical oceanography, the medium changes over time. M. Cowman *et al.* [11] adapted the diffusing wave spectroscopy technique [12] to acoustic waves in order to relate the temporal field fluctuations with the dynamics of the multiple scattering medium. J. D. Rosny and P. Roux [13] used the multiple scattering theory to measure the density and the scattering

strength of moving scatterers inside a highly reverberating cavity. They apply this theory to fish counting in a tank, but it can also be used to estimate its volume, the sound velocity, the absorption cross-sections, and other properties. A few months later, a parallel is established between these results and the diffusing acoustic wave spectroscopy [14, 15]. Excellent agreement is found between experiment and theory for steels balls moving in a water tank. Failing to accurately model the wave propagation in the random heterogeneous medium, some methods use it as an interferometer. The idea is to compare the response of the inspected medium before and after a change has been introduced. Thereby, the major part of the incoherent field is eliminated. Nevertheless, the residual coherent field can lead to detect, locate, or characterize a perturbation [16]. This technique can be useful in warning mode, or in the detection of temporal changes in the medium. Coda wave interferometry is an example of this type of method. It was used to estimate the variations in the positions of small changes in granite from multiply scattered waves by cross-correlating perturbed and unperturbed field [17]. Other studies use this method to detect larger changes [18] or to determine the relative location of earthquakes [19]. Despite their noisy and chaotic appearance, coda waves are highly repeatable. If a perturbation occurs, even if very small, an observable change will be produced in the coda waves. Thereby, the coda wave interferometry is able to determine the average motion of scatterers or change in the propagation velocity from the temporal change of multiply scattered waves. However, it cannot determine the exact location or the spatial extent of the change in the medium [20]. Inspired by coda wave interferometry C. Pacheco, and R. Snieder [20] use it in conjunction with a diffusive model to obtain an expression that relates the mean travel time change of multiply scattered waves with the localized perturbation in the propagation velocity of the medium. E. Larose *et al.* [21] use the coherent field part to formulate an inverse problem which is solved by a maximum likelihood approach in order to image and locate a weak perturbation in concrete. S. T. Rakotonarivo *et al.* [22] backpropagate the coherent field in a homogeneous reference medium in order to focus it on the position of the defect. In the latter application, the medium background is known. Only the heterogeneities nature and localization are unknown. These two studies are supported by conclusive experiments. However, the target must be approximately the same size as the heterogeneities of the medium in order to be correctly imaged.

1.2. Imaging methods for known heterogeneous media

In the situations where all geometrical and physical properties of the inspected medium are known, several methods allows performing NDT. Time-reversal exploits the reciprocity of wave equations to refocus an incident wavefield, measured by an array of transmit-receive transducers, to the location of the original source, regardless of the complexity of the propagation medium. Therefore, NDT is still possible, even with very dense cluttering as long as the full Green function is known [23]. The use of time reversal in imaging of cluttered media is also made in [24, 25] and in [26] for electromagnetic waves applications. The sensitivity of the refocusing properties of the time-reversed waves to the Green function accuracy is studied in [27, 28]. Usually, sufficiently accurate knowledge of the media is out of reach in many applications. Borcea *et al.* [29] use the principle of time-reversal in order to estimate the location of small scatterers in a randomly heterogeneous medium. The resulting imaging methods are based on the computation of an objective functional whose maxima are an estimation of the location of the scattering objects. This method is efficient if the number of inclusions is less than the number of transducers composing the array. The more the inclusions are separated, the more accurate the localization is. This approach leads to imaging methods such as MUSIC [30] and SAT [29]. Topological optimization was first developed to solve static structural inverse problems. It was then transposed to acoustics [31] and elastodynamics [32]. The parameter to be optimized is the location of an object in the structure. This object can be penetrable or a Dirichlet or a Neumann border inside the medium. Similarly to the Full WaveForm Inversion [33] where the variables to be optimized are continuous parameters of the medium (wave speed, density...), addressing the inverse problem implies the definition of a cost function and the study of its sensitivity to the optimized parameters. In topological optimization, this sensitivity is also referred as the topological gradient. It is a space dependent variable that takes high magnitude negative values where the insertion of the object will tend to strongly decrease the cost function. When looking for small Dirichlet or Neumann objects in a medium, simple analytical formulations are obtained as functions of two wavefields that are to be computed in the defect-free reference medium [34]. Similar formulas are also derived in Full Wave inversion when optimizing the inverse of the squared wave velocity [35]. Using these observations, the topological gradient (or one of its derivative) can be used as the imaging function [36] and is obtained with two numerical computations performed in the defect-free medium. This corresponds to the so

called topological imaging. Topological Imaging (TI) is thus a non-iterative process that is able to take into account the complexity of a medium through those two numerical simulations whose boundary conditions depend on the experimental excitation and measurements respectively. It has been applied to strongly dispersive waves [37] as well as to reverberating [38] and bounded media [39, 40]. It is shown with numerical experiments that defects are localized in anisotropic homogeneous [41] and anisotropic heterogeneous media [42]. Bellis and Bonnet also showed that cracks and their orientation could be retrieved in shells using the topological optimization approach [43].

1.3. Outline

The inspection of heterogeneous media covers a wide application field. When the effect of the heterogeneity on the acoustic field is small in comparison to the effect of the defect or easy to distinguish from, classical delay and sum methods allow appropriate imaging. Still, there are cases where neglecting the heterogeneity lead to strong artifacts or prevent from defect detection or medium characterization. For instance, weld inspection [42] or multi-material stratified media require the heterogeneity to be taken into account for accurate defect location. In vivo bone characterization [44] is another example where taking the heterogeneity into account allows previously unreleased medium characterization. In the present paper, a more academic example is chosen in order to assess the approach validity with a demanding test case, to compare the effect of choosing different reference media and to propose an imaging function compatible with fluid-solid media. The authors believe this could also be a first step toward phononic crystal nondestructive evaluation. The work focuses on Nondestructive Testing (NDT) applications through active ultrasonic imaging processes. Our aim is to apply the TI method to a known heterogeneous fluid-solid medium whose heterogeneities are arranged in an even manner. The defect to be localized is not an object but the absence of one of the heterogeneities. The paper is divided into four section. Section 2 explains the principle of TI and the way it is here applied to a known heterogeneous medium. The specimen under study and the numerical approach to model the acoustic wave propagation are described in detail. Depending on how accurately the medium is known, three different imaging methods are proposed. In section 3, the experimental apparatus and the imaging results obtained with synthetic and with experimental data respectively are presented and analyzed. Finally, applications and limitations of the techniques are discussed in section 4.

2. Applying topological imaging to a known heterogeneous medium

2.1. The topological imaging framework

The topological imaging process consists first in an active acoustic investigation of the medium, then in computing two specific wavefields and finally in computing the imaging from both wavefields. The wavefields are computed in a reference medium that includes all the knowledge of the medium, except the possible defects. Some known acoustic sources generate waves propagating and interacting with the medium and some known sensors measure the acoustic response. This corresponds to the step described in Fig. 1a. Then, this response is simulated in the reference medium, *i.e.* in the absence of defect (Fig. 1b). Finally, the residue is obtained as the difference between the two (Fig. 1c). This corresponds to the acoustic signature of the defect.

The two required numerical wavefields correspond to the solutions of the direct and adjoint prob-

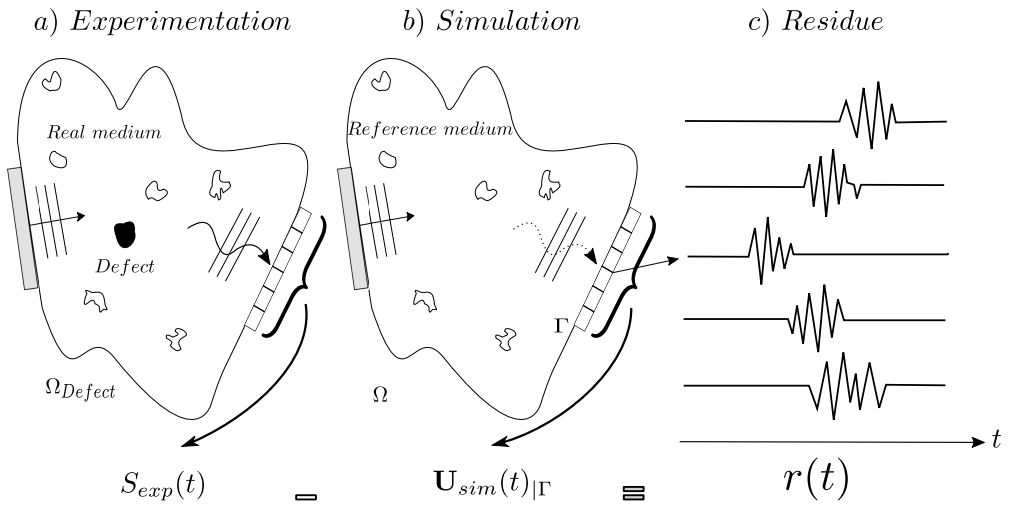

Figure 1: The active ultrasonic inspection for residue computation. (a) Experiments: acquisition of the response of the perturbed medium $S_{exp}(t)$. (b) Simulation: computation of the response of the reference medium at the transducer location $U_{sim}(t)$. (c) Residue: difference between experimental and simulated signals $r(t)$.

lems respectively. The direct problem consists in simulating the measurement in the defect-free medium. The experimental acoustic sources and sensors are thus simulated within the reference medium. Two steps of the process use the solution of the direct problem. First the experimental signals are compared to the simulated measurement, and their difference is defined as the residue.

Second, the whole space- and time- or frequency-dependent wavefield is stored to be used in the image computation. The adjoint problem consists in simulating the backpropagation of the residue from the measuring sensors in the same reference medium as the one used in the direct problem. The image is then obtained by computing a zero-lag convolution of direct and adjoint wavefields (Fig. 2).

It has to be emphasized that residue computation may be difficult when the wave response of the reference medium is complex. In the topological optimization approach, the residue is defined as the difference between a measured signal and a numerical simulation. This implies a quantitative measurement which is not easy when using for instance piezoelectric sensors. An alternative when available is to make a measurement before damaging the medium. It corresponds to the defect-free medium response and is used in residue computation to replace simulation [38].

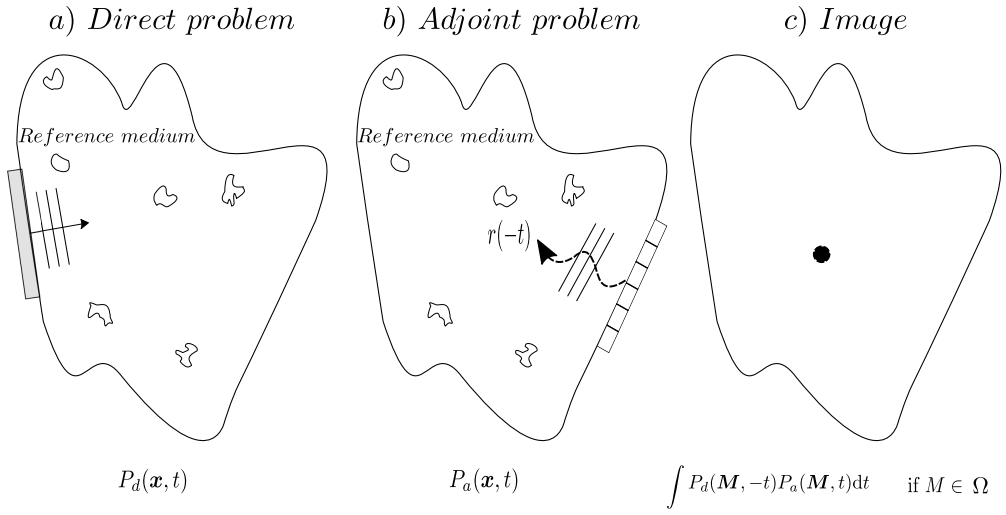

Figure 2: Formation of the image with topological imaging method. (a) Computation of the direct field. (b) Computation of the adjoint field. (c) Image computation.

2.2. The specimen under study

The specimen under study is a fluid-solid periodic cluster. This medium is made up of 275 steel rods immersed in water. The steel rods are arranged in an even manner forming a rectangle of 11 rows and 25 columns. The inter-row space and the inter-column space are 9.6 and 11.9 mm respectively. As the diameter of each rod is one millimeter, the surface concentration of the solid inclusions in the water is $C \simeq 0.7$ %. The elastic properties of steel are given by:

$E = 210.10^9$ Pa for Young's modulus, $\rho_{steel} = 7900$ kg/m^3 for density and $\nu = 0.285$ for the Poisson coefficient. That corresponds to a longitudinal wave velocity $c_L = 5902$ m/s and a transversal wave velocity $c_T = 3236$ m/s. During the physical experiment, the water temperature was 19.8°C, which implies that the velocity of the longitudinal waves is $c_{water} = 1477$ m/s and that the density is $\rho_{water} = 998$ kg/m^3.

2.3. Definition of the reference medium and the three corresponding imaging methods

Defining the reference medium is an important step of the method as it embeds all the knowledge of the medium that we want to be taken into account in the final image. In the present application, the natural choice is to simulate the steel bar cluster immersed in water assuming the locations of the bars and of the transducers are known. Thus, the reference medium is made of steel bars immersed in water and the transducers are facing the cluster according to the experiments. It correspond to what is here defined as heterogeneous TI.

Nevertheless, the case where the steel bars are not taken into account is also studied. In this second case, the reference medium is simply a semi-infinite water medium. This medium is of interest as it corresponds to the one implicitly considered when applying classical delay and sum methods. Delay and sum and topological methods have some physics in common. It is shown in the Appendix that assuming a homogeneous infinite and single-polarization reference medium, applying topological imaging allows retrieving the classical delay and sum method imaging function. This case corresponds to what is here defined as homogeneous TI.

It has to be reminded that the reference medium is used for both direct and adjoint field and that direct field is used for both residue and image computation. That's why an alternative method is also studied. It consists in taking a reference medium for residue computation and another one for direct and adjoint fields that are necessary in image computation. In the present case, the hybrid method consists in measuring the experimental residue by substracting the measure obtained in the experimental defect free medium with that obtained in the real medium. Thus, the heterogeneity of the medium is fully taken into account in the residue computation. Hence, the reference medium is the heterogeneous medium. Then the experimental information (transducer excitation and residue) is used to compute direct and adjoint fields in a homogeneous reference medium. It has to be noted that this method is similar to that described by Rakotonarivo *et al.* [22]. To sum up, three methods are here tested: the heterogeneous, the homogeneous and the

hybrid TI methods (see Table 1).

	Reference Medium		Caption
	for residue	for direct & adjoint fields	
Heterogeneous TI	Heterogenous	Heterogeneous	
Homogeneous TI	Homogeneous	Homogeneous	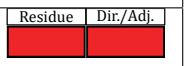
Hybrid TI	Heterogenous	Homogeneous	

Table 1: The imaging methods compared in this study. This table specifies the reference media used to obtain the images for each method.

2.4. Numerical modelling

The experiments are performed in three-dimensional space at a central frequency of 500 kHz. The steel rods are all oriented along the $\mathbf{x}_3$ axis and so is the length of the transducers. All have large dimensions in comparison to the wavelength in water. Thus the propagation is assumed two-dimensional. The propagation space is noted $(\mathbf{x}_1, \mathbf{x}_2)$ whereas the third dimension is noted $\mathbf{x}_3$ (Fig. 3). The plane strain assumption is applied along $\mathbf{x}_3$. Numerical simulations are performed using frequency-domain finite elements in the 200 to 800 kHz bandwidth with the COMSOL Multiphysics software[2]. Plane elasticity equations model the wave propagation in the fluid-solid periodic cluster. The scalar wave equation is used in water and the vectorial equations are applied in the steel rod sections. The continuity of normal displacements and normal stresses at the fluid/solid interfaces is managed by the Multiphysics module of COMSOL software. The excitation source corresponding to each transducer is modelled with normal velocity conditions applied at the boundary of the medium. The semi-infinite nature of the medium is modeled by absorbing regions similar to those defined in [45]. The absorbing region is defined as a region where the imaginary part of wave velocity is progressively increasing in order to generate progressively increasing absorption. Simultaneously, the density is modified so that the acoustic impedance is constant to achieve minimal reflection. This method is especially suited to solid anisotropic media where PMLs are

[2]http://www.comsol.com

harder to apply. Still it is also efficient in fluids. In this application, the thickness of the absorbing region is three times the largest wavelength which is about 7.4 mm. The same mesh is used for all computation frequencies. It is clear to the authors that this is not optimized but it eases the processing and avoids re-meshing at each frequency. The mesh is composed of quadratic triangular elements carrying second-order polynomial interpolation functions. The minimal size of an element is taken as a fourth of the shortest wavelength. This would correspond to the eight of the shortest wavelength using linear interpolation functions. The shortest wavelength is obtained at 800 kHz. Thus, at the central frequency of 500 kHz, the mesh elements are smaller than a sixth of the wavelength. This compromise was found to ensure low numerical dispersion.

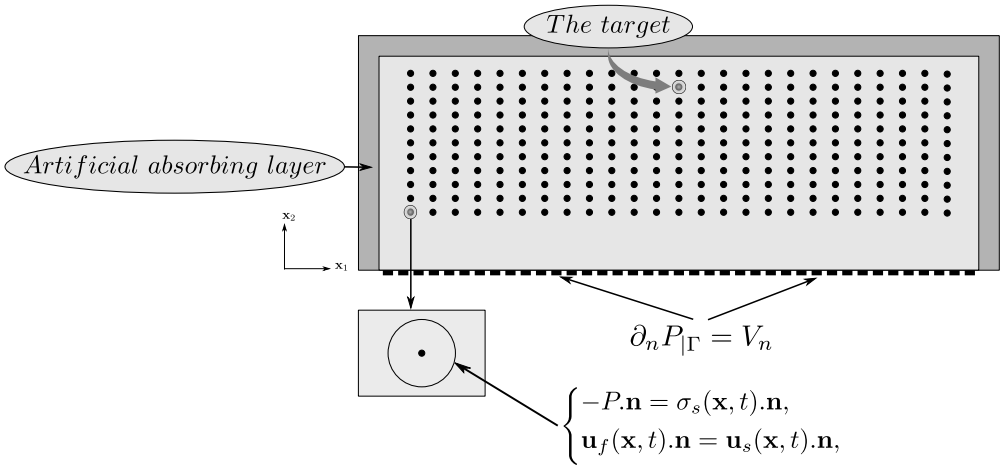

Figure 3: Numerical model of the wave propagation in the investigation environment. The ultrasonic probe is represented by the bold broken line at the bottom of the rectangle. On the one hand, the light gray rectangle represents water. On the other hand, the dark gray rectangle represents the artificial absorbent layer. The black discs represent the steel rods composing the periodic cluster. The target is buried deep in the periodic cluster, located at the intersection of 13th column and 10th row.

2.5. The imaging function

Following the topological imaging approach, the imaging function is defined as the norm product between direct and adjoint wavefields integrated over the frequency domain. It can also be obtained in the time-domain by taking the spatial envelope of the zero-lag convolution between both fields

[37]. The specificity of present application is that the medium is made of fluid and solid. On the one hand, the numerical degree of freedom is the hydrostatic pressure P_f. On the other hand, it is the displacement vector $\mathbf{u_s}$. The common physical variable chosen to compute the image is the isostatic pressure noted P. It is expressed as:

$$P = \begin{cases} P_f(\mathbf{x}) & \text{if } \mathbf{x} \in \text{fluid} \\ -\frac{1}{2}\text{Tr}\left(\sigma_{\mathbf{s}}(\mathbf{x})\right) & \text{if } \mathbf{x} \in \text{solid} \end{cases} \tag{1}$$

where Tr is the trace function and $\sigma_{\mathbf{s}}(\mathbf{x})$ is the 2D stress tensor. Thus, the image is simply given by:

$$I(\mathbf{x}) = \left| \int_{\mathbb{R}^+} P_d(\mathbf{x},\omega) P_a(\mathbf{x},\omega) d\omega \right| \tag{2}$$

where $P_d(\mathbf{x},\omega)$ and $P_a(\mathbf{x},\omega)$ are the isostatic pressure fields in direct and adjoint wavefields respectively. This definition is used for both pure fluid and fluid-solid reference media.

3. Theoretical and experimental results

This section is dedicated to the images of the test-specimen obtained with the three different methods of Table 1. In what follows, the target is not an object but the absence of the rod located in the 13th column and the 10th row of the cluster (Fig. 3). First, the experimental setup is described, then the results obtained with synthetic and experimental data are presented for each imaging method listed in Table 1.

3.1. The experimental apparatus

The experimental apparatus is presented Fig. 4. The cubic structure presented in the front view (Fig. 4a) is composed of two horizontal thin steel plates. The plates are identical and perforated according to a known periodic geometric pattern in order to hold the steel bars vertically. Each of them is clamped between two thick PVC plates making the setup stiff and stable. To inspect the medium in a pulse-echo configuration, an Imasonic ultrasonic transducer array is placed in front of the medium of investigation, at a distance a=37 mm. In addition, the probe is centered relative to the periodic cluster of steel rods and is parallel to its first row similarly to Fig. 3. The ultrasonic array is composed of 128 programmable transmitters/receivers with a 500 $\pm$ 10 KHz central frequency, the acoustic adaptation layer mechanical impedance is 3.2 MRayl. Each array element is 2 mm wide and the array pitch p is 2.5 mm, which makes a total active length of 319.5

mm. The transducer array is connected to a multi-channel Lecoeur Electronique measurement system. This device is used at a 10 MHz sampling frequency. Note that the experiments take place in a water tank as shown in the perspective view (Fig. 4b).

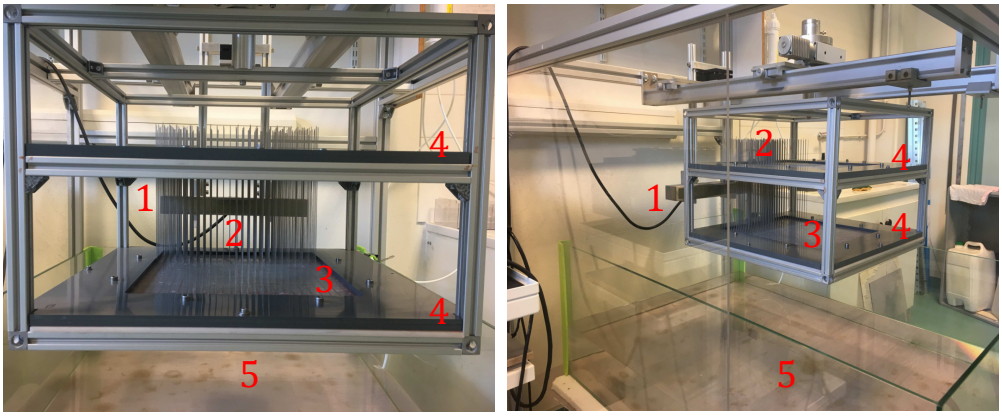

(a) (b)

Figure 4: The experimental setup and the specimen under study before immersion. (a) Front view. (b) Perspective view . (1) The ultrasonic transducers array. (2) The periodic cluster of steel rods. (3) The perforated steel plates. (4) The PVC plates. (5) The water tank.

For each measure, the medium is insonified once by firing simultaneously all transducers with the same three-period windowed sinusoidal signal in order to generate a quasi-plane wave. This choice is not a restriction, any known excitation signal can be used. The residue that compares the response of the unperturbed medium with the response of the perturbed medium requires two acquisitions. The first one is the response of the medium with all the rods of the periodic cluster. The second one is the response of the medium after removing the rod. A typical experimental waveform is plotted Fig. 5. The backscattered wave is complex, as it combines the simple scattering contribution and the multiple scattering contribution. First 11 wave packets corresponding to the rows of the periodic cluster can be distinguished inside rectangle 2. The signal part in rectangle 3 is the superimposition of late arrival partial waves. The later the wave arrives, the more multiple scattering it underwent and the more it explored the medium. Rectangle 1 corresponds to the saturation of the receiving channel during emission as it is also used to generate the acoustic wave. In practice, the electrical excitation signal is distorted at the output of the transducers as the piezoelectric transducers have their own transfer function. Consequently, the acoustic wave generated does not correspond exactly

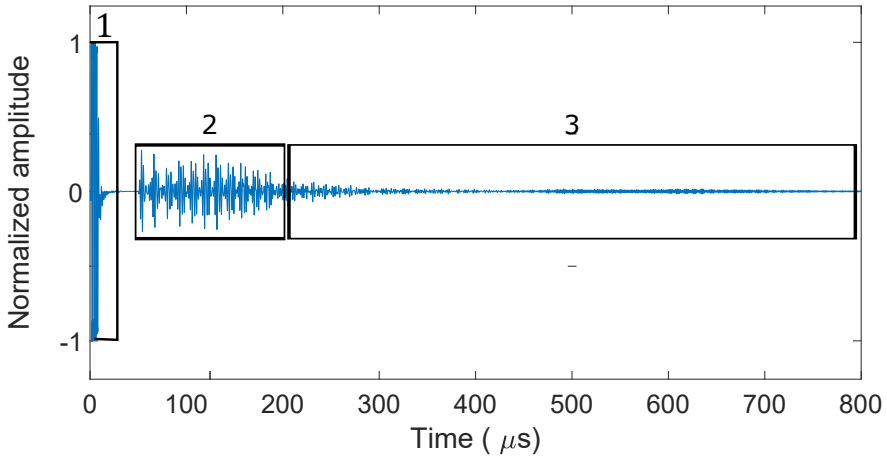

Figure 5: Typical normalized experimental signal.

to the electrical excitation signal. In the simulations the piezoelectric behaviour of the transducers is here not simulated. Thus, the normal velocity signal applied to the boundary of the medium (Fig. 3) should be proportional to the generated pressure signal. In order to identify this excitation signal, a calibration of the physical experience is performed so that experimental and numerical simulation are in accordance. The excitation signal obtained is presented Fig. 6.

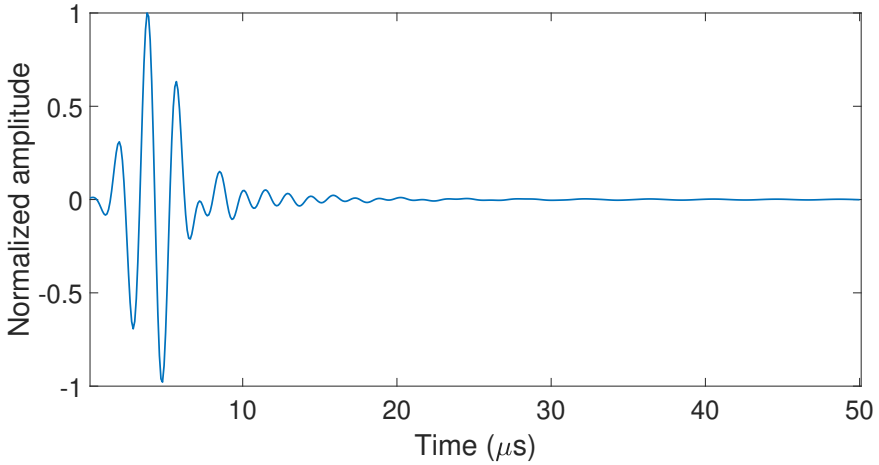

Figure 6: The experimental excitation signal

3.2. Results

The imaging methods presented in Table 1 are tested using successively synthetic and experimental data. The difference lies in the way the measured signals are obtained, either with simulations or with experiments respectively. The experimental data are obtained using the ultrasonic acquisitions of the real medium, in the absence and in the presence of the defect. This data is then used to calculate the residue and to compute the adjoint problem associated with each method. The synthetic data are obtained by computing the propagation of acoustic waves in the virtual defective medium and in the virtual defect-free medium. Then, the residue is used to compute the adjoint problem according to the method studied. The direct and the adjoint fields are computed in the frequency domain according to the numerical model introduced in paragraph 2.4. The results obtained with the three methods described in Table 1 are successively presented.

3.2.1. Heterogeneous TI results

In heterogeneous TI, the heterogeneous reference medium is used to calculate the residue, the direct, and the adjoint fields. Therefore, the residue contains the ballistic wave corresponding to the defect (here, the absence of a rod) and the corresponding multiple interactions with the other inclusions of the periodic cluster. On the one hand, the direct problem corresponds to the simulation of the physical experiment in the defect-free medium (the one containing all the rods). On the other hand, the adjoint problem corresponds to the backpropagation of the residue from the measurement surface in the defect-free medium. The imaging function is normalized. Thus it is defined by $I(\mathbf{x})/\max(I(\mathbf{x}))$ where $I(\mathbf{x})$ is given by Eq. (2). The images obtained with synthetic and experimental data are presented Fig. 7(a) and (b) respectively. The defect appears as a single point. Artefacts are small so that no wrong defect detection is likely to occur. In the zoom dial, the white circle indicates the true edges of the missing rod (the defect) in the medium. The spot maxima are located at the lower edge of the defect. This can be explained by the single insonification coming from the bottom that implies that the lower edge of the defect is more insonificated than the rest of the defect. In both cases, the defect is accurately located and no artefacts could indicate a defect where there is none.

The -6dB width of the spots is about 1.7 and 1.8 mm for the synthetic and the experimental data cases respectively. These values correspond to $0.57\lambda_0$ ans $0.6\lambda_0$ where λ_0 is the wavelength in water at the central frequency 500 kHz. Such a high resolution is achieved with a single insonification.

This can be explained by the fact that topological imaging takes the complex nature of the medium into account. It thus takes advantage of the enhanced refocusing properties of the time reversal operation in such media when computing the adjoint field.

The spot of the experimental data based image is a little off the defect and a secondary spot is present. They can be explained by a small transducer array location estimation in the experiments.

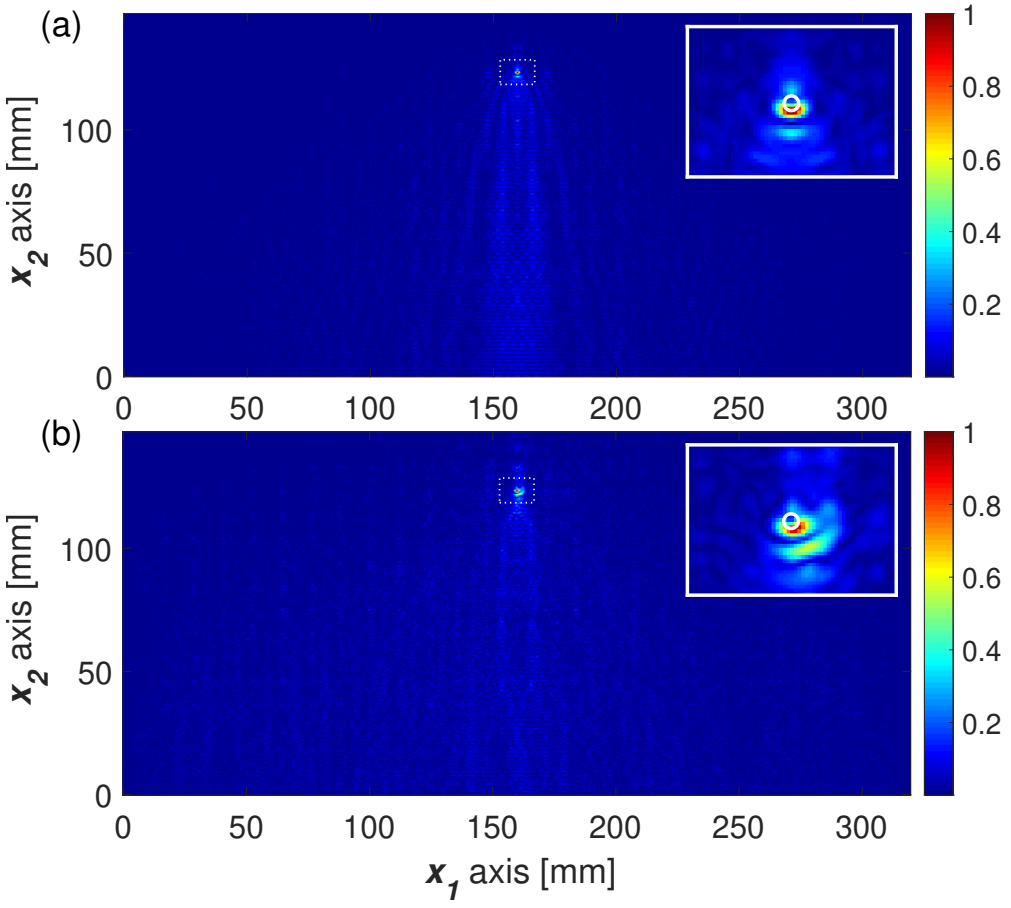

Figure 7: 

Images obtained with heterogenous TI and with: (a) synthetic data, (b) Experimental data. The real defect is delimited by the white hollow circle.

3.2.2. Homogeneous TI results

In homogeneous TI, the heterogeneity of the medium is taken into account neither in the residue computation, nor in the direct and adjoint fields computations. The direct problem corresponds

to the propagation of a quasi-plane wave propagating in a homogeneous semi-infinite medium. The adjoint problem corresponds to the backpropagation of the pressure field measured in the experiments into the same homogeneous semi-infinite reference medium. The imaging function is given by $I(\mathbf{x})/\max(I(\mathbf{x}))$. The images obtained with synthetic and experimental data are presented Fig. 8(a) and (b) respectively. As the rods are not in the reference medium, they all corresponds to perturbations and should thus appear as defects in the image. In practice, resolution and contrast decrease with the investigation depth so that the rods of first six rows can be identified but deeper, the image is poorly defined. In the image obtained with synthetic data (Fig. 8(a)) the last three rows are too blurry to make any sure conclusion about the presence or the absence of the rods. In the image obtained with experimental data (Fig. 8(b)), the missing rod can be better identified but wrong missing rod detection occur elsewhere. It is shown in appendix 4 that in this case, topological imaging is similar to classical delay and sum methods. As a conclusion, when not taking the heterogeneity of the medium in the reference model, some defect may thus be missed or detected even when not existing.

It should be noticed that the image obtained with the synthetic data (Fig. 8(a)) looks nosier than that obtained with experimental data (Fig. 8(b)). This can be explained by a discrepancy between synthetic and experimental apparent attenuation when measuring the acoustic field reflected by the rods. As a matter of fact, experimental signals are attenuated in a shorter time than synthetic signals. That means that synthetic data contain more multiple interactions between the rods themselves and between the rods and the transducer boundary than the experimental data. Thus, when considering a reference medium that is too different from the one investigated, the artifacts are stronger. This explains the nosier look of the image when using the homogeneous reference medium. The discrepancy between synthetic and experimental apparent attenuation can be explained by several phenomena. First, the transducer array is neither generating a perfect plane wave nor a perfectly collimated wave field and the induced diffraction in the $\mathbf{x}_3$ axis is not taken into account in the 2D-model used to generate the synthetic data. A second possibility is that despite our efforts, the rods may not be perfectly normal to the incident wave field. This could imply some more diffraction along the $\mathbf{x}_3$ axis.

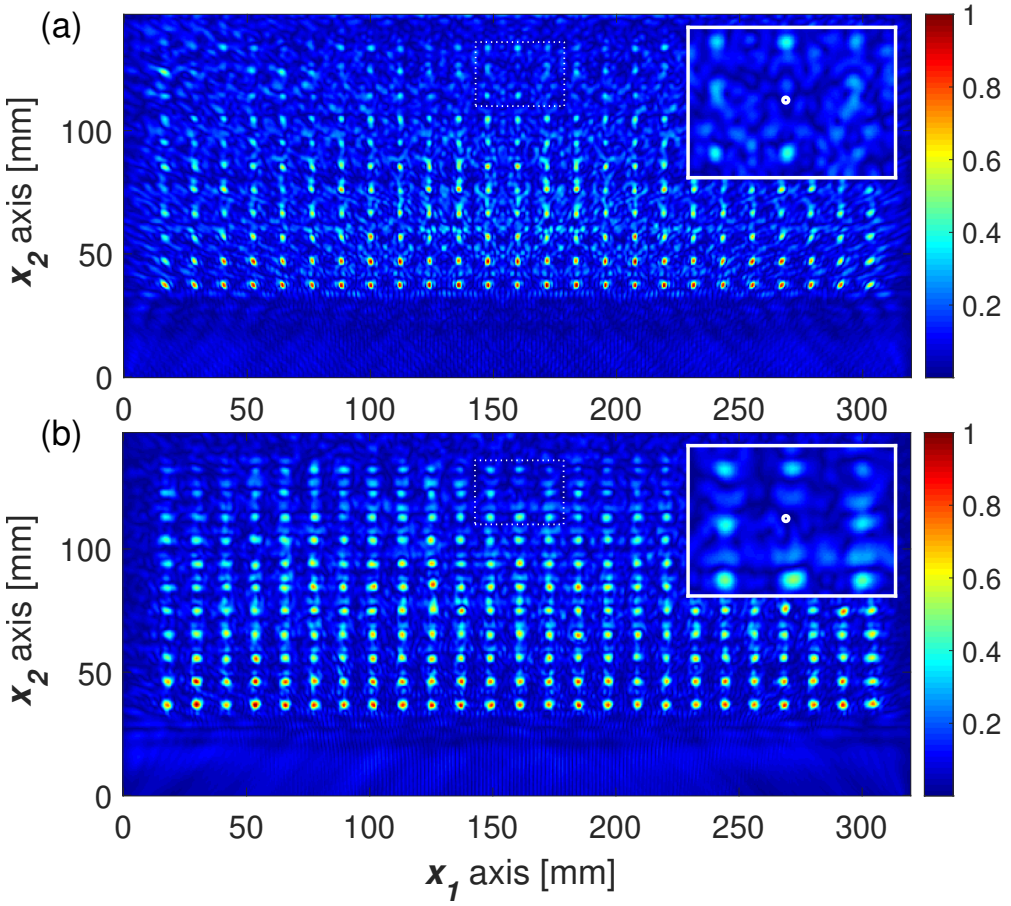

Figure 8: Images obtained with homogeneous TI and with: (a) synthetic data, (b) Experimental data. The real defect is delimited by the white hollow circle.

3.2.3. Hybrid TI results

The implementation of this hybrid TI method requires two distinct reference media. The first reference medium used to calculate the residue is heterogeneous. The second reference medium in which the direct and adjoint fields are calculated is homogeneous. The spot in the images indicate accurately the location of the defect and no misinterpretation is possible like in homogeneous TI. When processing the synthetic data, the defect and the corresponding spot are superimposed in the image. When processing the experimental data, the spot is shifted 1.1 mm to the right and 0.8 mm to the front. We interpret this error as an array location estimation error. We consider it as small in comparison to the wavelength in water at the central frequency $\lambda_0 = 3$ mm and to the active size of the array (320mm). The -6dB width of the spot is respectively 2.5 mm and

3.5 mm for the synthetic data and the experimental data image. They corresponds to $0.83\lambda_0$ and to $1.16\lambda_0$ respectively which are very reasonable values for a one-insonification image. The spots are clearly wider than those in the heterogeneous TI images. Taking into account the complexity of the medium in the Heterogeneous TI gives better focusing in the backpropagation and thus a better resolution in the image. This observation corroborates the results demonstrated in [23].

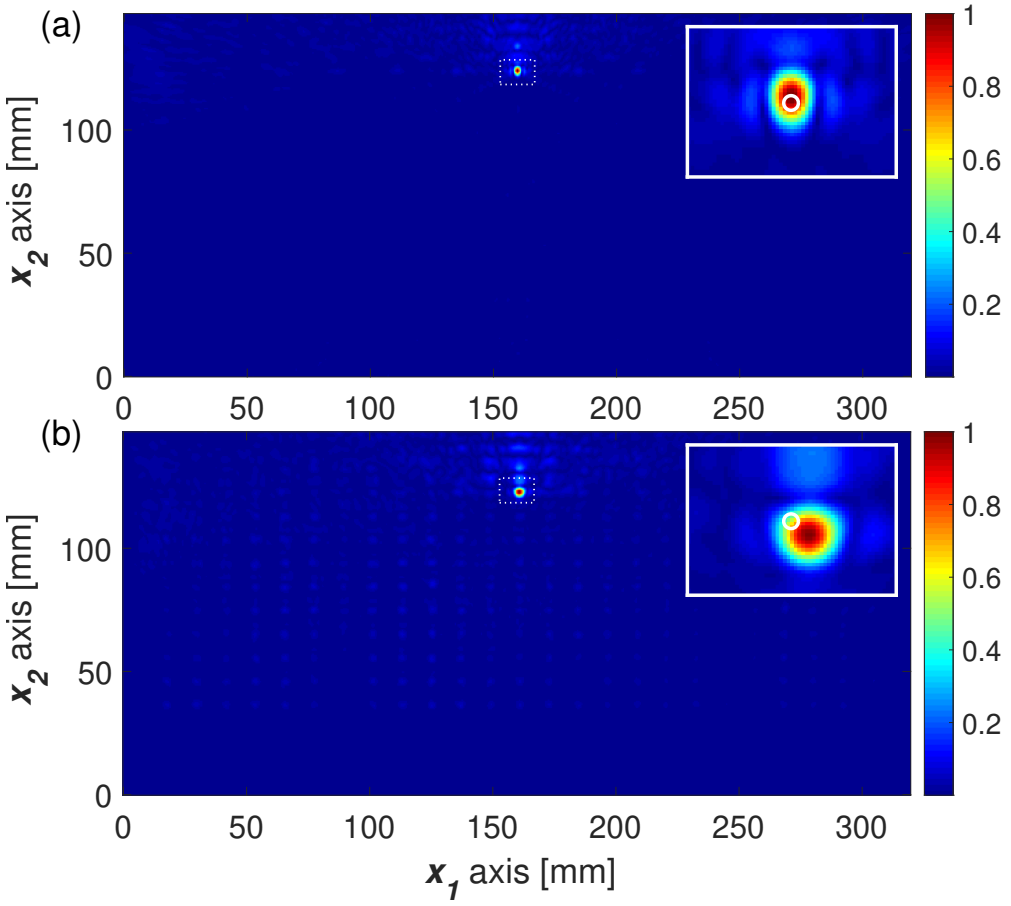

Figure 9: Images obtained with hybrid TI and with: (a) synthetic data, (b) Experimental data. The real defect is delimited by the white hollow circle

4. Discussions and conclusions

The same heterogeneous medium is studied following three different methods, all deriving from the topological imaging approach. The defect to be located is here the absence of one of the elements

constituting the periodic cluster. The topological imaging framework allows the heterogeneous complex nature of the defect-free medium to be taken into account in the imaging process. This corresponds to the so called heterogeneous topological imaging. It allows an accurate location of the defect both when applying it to synthetic or to experimental data. When ignoring the heteroeneous nature of the medium, the reference medium used to build the image is homogeneous. Thus, all cluster elements should appear as defects in the image. In practise, the first rows are accurately described but the resolution and contrast decrease with the investigation depth so that the missing element is hardly located and wrong defect detection may occur. It is demonstrated that the so called homogeneous topological imaging is in fact similar to classical delay and sum methods. In the hybrid topological imaging method, the heterogeneous nature of the defect-free medium is only required for the residue measurement. It allows accurate location of the defect at the cost of a degraded resolution in comparison with the heterogeneous TI. It has to be noted that hybrid TI is in fact similar to the method presented in [22]. The advantage is that the wavefields required to obtain the image are computed in a homogeneous medium which allows fast computation methods. Still, in both, hybrid and heterogeneous TI, experimental residue is in practise required which implies that the experimental acoustic response of the defect-free medium has to be known.
The medium investigated here present a small inclusion concentration. This work is a first step towards more concentrated media investigation in order to prepare phononic crystal nondestructive testing.

Acknowledgments

This work was funded by the french Ministry of Higher Education, Research and Innovation.

Appendix: Equivalency between Delay and Sum methods and homogeneous Topological imaging in infinite media

In this appendix, it is demonstrated that the delay and sum imaging function can be retrieved from the application of topological imaging method to an homogeneous infinite medium. For pedagogical purposes, the calculation is performed in the time domain. It could also be done in the frequency domain.
Let us consider a homogeneous infinite fluid medium characterized by the wave velocity c and let

us apply the topological imaging method to this medium. The transducer network consists of N transducers located at $\mathbf{t}_i$ on the $\mathbf{x}_1$ axis, where $1 < i < N$ (Fig. 10). The emitted and received signals are noted $e(t)$ and $s_i(t)$ respectively. In the topological framework, the residue is defined as the difference between responses obtained in the defect free medium and that in the presence of possible defects. In a homogeneous infinite medium, no signal is measured in the absence of defect as waves propagate to infinity. Thus, in that case, residue signals are simply the measured signal. In that context the infinite medium hypothesis simply implies that the boundaries of the domain are sufficiently far away regarding the acquisition duration. Let $h(\mathbf{t}_e, \mathbf{x}, t)$ be the impulse response between a source located at $\mathbf{t}_e$ and any given point $\mathbf{x}$. Depending on the type of insonification the distance d_f traveled by the wave to reach point $\mathbf{x}$ is given by:

1. $d_f = \| \mathbf{x} - \mathbf{t}_e \|$ if a single transducer is used to insonify the medium.
2. $d_f = \| \mathbf{n}.\mathbf{x} \|$ if a plane wave is used (given by the direction $\mathbf{n}$). The direction of the wave front is typically obtained applying appropriate delay laws to $e(t)$.

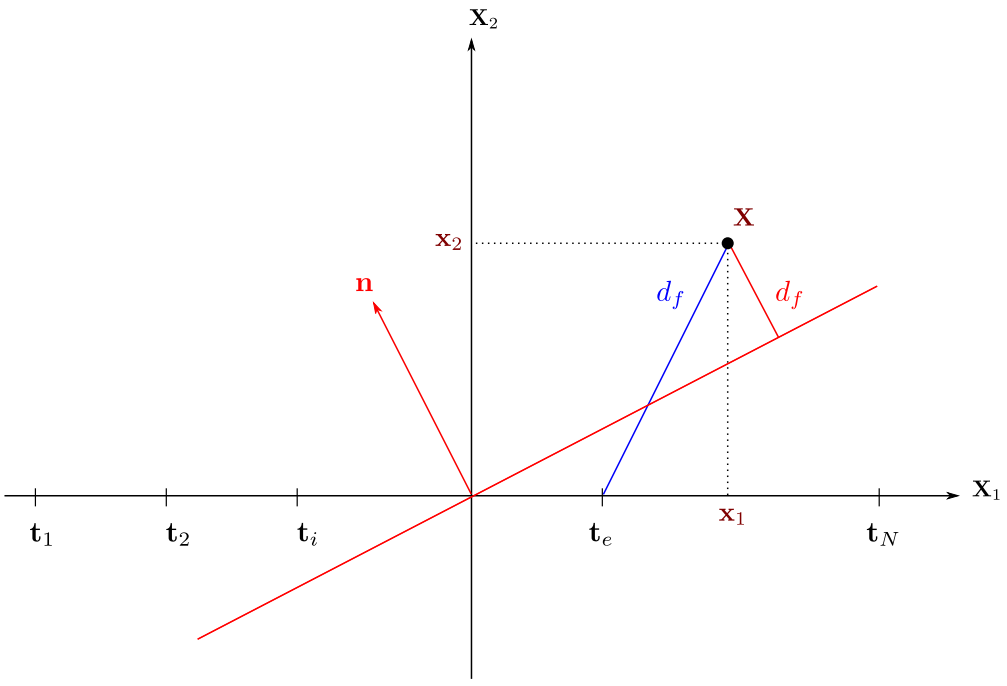

Figure 10: Schematic representation of medium and excitation types. The red line represents the wave front generated by all the transducers and given by the direction $\mathbf{n}$. The blue line represents the excitation by a single transducer located at $\mathbf{t}_e$.

The imaging function of topologcial imaging is given by the spatial envelope of the function $\mathcal{I}(\mathbf{x})$ written as:

$$\mathcal{I}(\mathbf{x}) = \int_{-\infty}^{\infty} \mathbf{u}(\mathbf{x},t)\mathbf{v}(\mathbf{x},-t)dt, \tag{3}$$

where $\mathbf{u}$ and $\mathbf{v}$ are the solutions of the direct and the adjoint problems respectively. According to the type of insonification, the direct field takes one of the following two forms:

1. A single emitter located at $\mathbf{t}_e$:

$$\mathbf{u}(\mathbf{x},t) = \left[e * h\left(\mathbf{t}_e, \mathbf{x}, \bullet\right)\right](t), \tag{4}$$

2. A plane wave front propagating in direction $\mathbf{n}$:

$$\mathbf{u}(\mathbf{x},t) = \left[e * \delta\left(\bullet - \frac{\mathbf{n}.\mathbf{x}}{c}\right)\right](t). \tag{5}$$

The adjoint field is given by:

$$\mathbf{v}(\mathbf{x},t) = \sum_{i=1}^{N_r} \left[s_i^* * h\left(\mathbf{t}_i, \mathbf{x}, \bullet\right)\right](t), \tag{6}$$

where $s_i^*(t) = s_i(-t)$ is the time reversed signal.

In the hypothesis of ray propagation, the impulse response is approximated by: $h(\mathbf{t}_e, \mathbf{x}, t) = \delta\left(t - \frac{\|\mathbf{x}-\mathbf{t}_e\|}{c}\right)$ regardless of the size or shape of the source. Therefore, the fields $\mathbf{u}$ and $\mathbf{v}$ are respectively expressed as follows:

$$\begin{aligned} \mathbf{u}(\mathbf{x},t) &= \left[e * \delta\left(\bullet - \frac{d_f}{c}\right)\right](t) \\ &= e\left(t - \frac{d_f}{c}\right), \end{aligned} \tag{7}$$

$$\mathbf{v}(\mathbf{x},t) = \sum_{i=1}^{N_r} \left[s_i^* * \delta\left(\bullet - \frac{\parallel \mathbf{x} - \mathbf{t}_i \parallel}{c}\right)\right](t). \tag{8}$$

The time reversed adjoint field is thus given by:

$$\mathbf{v}(\mathbf{x},-t) = \sum_{i=1}^{N_r} \left[s_i\left(t + \frac{\parallel \mathbf{x} - \mathbf{t}_i \parallel}{c}\right)\right]. \tag{9}$$

Inserting Eq. (7) and Eq. (9) in Eq. (3) leads to:

$$\begin{aligned} \mathcal{I}(\mathbf{x}) &= \int \mathbf{u}(\mathbf{x},t)\mathbf{v}(\mathbf{x},-t)dt \\ &= \int e\left(t - \frac{d_f}{c}\right) \sum_{i=1}^{N_r} \left[s_i\left(t + \frac{\parallel \mathbf{x} - \mathbf{t}_i \parallel}{c}\right)\right] dt \\ &= \int e(\tau) \sum_{i=1}^{N_r} \left[s_i\left(\tau + \frac{d_f + \parallel \mathbf{x} - \mathbf{t}_i \parallel}{c}\right)\right] d\tau, \end{aligned} \tag{10}$$

where $\tau = t - \frac{d_f}{c}$. Assuming that the emission signal is a Dirac impulse $e(t) = \delta(t)$, the function $\mathcal{I}$ is given by:

$$\mathcal{I}(\mathbf{x}) = \sum_{i=1}^{N_r} s_i \left(\frac{d_f + \parallel \mathbf{x} - \mathbf{t}_i \parallel}{c} \right), \tag{11}$$

As a matter of fact, $\mathrm{Env}(\mathcal{I}(\mathbf{x}))$ corresponds to the definition of the imaging function of the delay and sum method [2, 46]. This result can easily be generalized to any excitation with several emitters located at $\mathbf{x}_j$ and emitting with relative delays noted β_j. In this case, the imaging function is given by:

$$\mathcal{I}(\mathbf{x}) = \sum_{i,j} s_i \left(\frac{\parallel \mathbf{x} - \mathbf{t}_j \parallel + \parallel \mathbf{x} - \mathbf{t}_i \parallel}{c} + \beta_j \right). \tag{12}$$

Unlike conventional imaging methods, IT involves separate processing of transmitted and measured signals. Thus, the explicit computations of the distances between the emitters, the potential defect and the receiver are not carried out. They are implicitly taken into account in the two computation of direct and adjoint fields.

To sum up, assuming ray-tracing wave propagation, Dirac-like emission signals, the delay and sum imaging functions are retrieved from the topological imaging framework. Let us recall that delay and sum imaging function validity is limited to medium that are homogeneous and that can be considered infinite or semi-infinite (it is to say whose boundaries are far enough regarding the signal acquisition duration). Thus, topological imaging framework offers more general imaging heuristics as it can also be applied to bounded and heterogeneous media.

References

[1] J. Busse, Three-Dimensional Imaging Using a Frequency- Domain Synthetic Aperture Focusing Technique, IEEE Transactions on Ultrasonics, Ferroelectrics and Frequency Control 39 (2) (1992) 174–179 (1992).

[2] C. Holmes, B. W. Drinkwater, P. D. Wilcox, Post-processing of the full matrix of ultrasonic transmit â receive array data for non-destructive evaluation, NDT & E International 38 (2005) 701–711 (2005). doi:10.1016/j.ndteint.2005.04.002.

[3] R. Sicard, J. Goyette, D. Zellouf, A SAFT algorithm for lamb wave imaging of isotropic plate-like structures, Ultrasonics 39 (7) (2002) 487–494 (2002). doi:10.1016/S0041-624X(01)00087-7.

[4] M. Spies, W. Jager, Synthetic aperture focusing for defect reconstruction in anisotropic media, Ultrasonics 41 (2) (2003) 125–131 (2003). doi:10.1016/S0041-624X(02)00407-9.

[5] A. Leleux, P. Micheau, M. Castaings, Long range detection of defects in composite plates using lamb waves generated and detected by ultrasonic phased array probes, Journal of Nondestructive Evaluation 32 (2) (2013) 200–214 (2013). doi:10.1007/s10921-013-0173-0.

[6] G. Bal, O. Pinaud, Time-reversal-based detection in random media, Inverse Problems 21 (5) (2005) 1593–1619 (sep 2005). doi:10.1088/0266-5611/21/5/006.

[7] G. Bal, L. Carin, D. Liu, K. Ren, Experimental validation of a transport-based imaging method in highly scattering environments, Inverse Problems 23 (6) (2007) 2527–2539 (nov 2007). doi:10.1088/0266-5611/23/6/015.

[8] C. Prada, M. Fink, Eigenmodes of the time reversal operator: A solution to selective focusing in multiple-target media, Wave Motion 20 (2) (1994) 151–163 (1994). doi:https://doi.org/10.1016/0165-2125(94)90039-6.
URL http://www.sciencedirect.com/science/article/pii/0165212594900396

[9] A. Aubry, A. Derode, Detection and imaging in a random medium: A matrix method to overcome multiple scattering and aberration, Journal of Applied Physics 106 (4) (2009) 044903 (2009). arXiv:https://doi.org/10.1063/1.3200962, doi:10.1063/1.3200962.
URL https://doi.org/10.1063/1.3200962

[10] A. Aubry, A. Derode, Multiple scattering of ultrasound in weakly inhomogeneous media: Application to human soft tissues, The Journal of the Acoustical Society of America 129 (1) (2011) 225–233 (2011). arXiv:https://doi.org/10.1121/1.3506343, doi:10.1121/1.3506343.
URL https://doi.org/10.1121/1.3506343

[11] M. Cowan, I. Jones, J. Page, D. Weitz, Diffusing acoustic wave spectroscopy, Physical Review E 65 (2002) 066605 (Jun 2002). doi:10.1103/PhysRevE.65.066605.
URL https://link.aps.org/doi/10.1103/PhysRevE.65.066605

[12] D. J. Pine, D. A. Weitz, P. M. Chaikin, E. Herbolzheimer, Diffusing wave spectroscopy, Physical Review Letters 60 (1988) 1134–1137 (Mar 1988). doi:10.1103/PhysRevLett.60.1134.
URL https://link.aps.org/doi/10.1103/PhysRevLett.60.1134

[13] J. De Rosny, P. Roux, Multiple scattering in a reflecting cavity: Application to fish counting in a tank, The Journal of the Acoustical Society of America 109 (6) (2001) 2587–2597 (2001). doi:10.1121/1.1369101.
URL https://doi.org/10.1121/1.1369101

[14] D. Demer, S. Conti, J. De Rosny, P. Roux, Absolute measurements of total target strength from reverberation in a cavity, The Journal of the Acoustical Society of America 113 (3) (2003) 1387–1394 (2003). doi:10.1121/1.1542648.
URL https://doi.org/10.1121/1.1542648

[15] J. de Rosny, P. Roux, M. Fink, J. H. Page, Field fluctuation spectroscopy in a reverberant cavity with moving scatterers, Physical Review Letters 90 (2003) 094302 (Mar 2003). doi:10.1103/PhysRevLett.90.094302.
URL https://link.aps.org/doi/10.1103/PhysRevLett.90.094302

[16] S. Feng, D. Sornette, Acoustical nondestructive evaluation of heterogeneous materials in the multiple scattering regime, The Journal of the Acoustical Society of America 90 (4) (1991) 1742–1748 (1991). doi:10.1121/1.401654.
URL https://doi.org/10.1121/1.401654

[17] R. Snieder, A. Grêt, H. Douma, J. Scales, Coda wave interferometry for estimating nonlinear behavior in seismic velocity, Science 295 (5563) (2002) 2253–2255 (2002). doi:10.1126/science.1070015.
URL https://science.sciencemag.org/content/295/5563/2253

[18] O. Lobkis, R. Weaver, Coda-wave interferometry in finite solids: Recovery of p-to-s conversion rates in an elas-

todynamic billiard, Physical Review Letters 90 (2003) 254302 (Jun 2003). doi:10.1103/PhysRevLett.90.254302.
URL https://link.aps.org/doi/10.1103/PhysRevLett.90.254302

[19] R. Snieder, M. Vrijlandt, Constraining the source separation with coda wave interferometry: Theory and application to earthquake doublets in the hayward fault, california, Journal of Geophysical Research: Solid Earth 110 (B4) (2005). doi:10.1029/2004JB003317.
URL https://agupubs.onlinelibrary.wiley.com/doi/abs/10.1029/2004JB003317

[20] C. Pacheco, R. Snieder, Time-lapse travel time change of multiply scattered acoustic waves, The Journal of the Acoustical Society of America 118 (3) (2005) 1300–1310 (2005). doi:10.1121/1.2000827.
URL https://doi.org/10.1121/1.2000827

[21] E. Larose, T. Planes, V. Rossetto, L. Margerin, Locating a small change in a multiple scattering environment, Applied Physics Letters 96 (20) (2010) 204101 (2010). arXiv:https://doi.org/10.1063/1.3431269, doi:10.1063/1.3431269.
URL https://doi.org/10.1063/1.3431269

[22] S. T. Rakotonarivo, S. C. Walker, W. A. Kuperman, P. Roux, Localization of a small change in a multiple scattering environment without modeling of the actual medium, The Journal of the Acoustical Society of America 130 (6) (2011) 3566–3573 (2011). arXiv:https://doi.org/10.1121/1.3652859, doi:10.1121/1.3652859.
URL https://doi.org/10.1121/1.3652859

[23] A. Derode, P. Roux, M. Fink, Robust acoustic time reversal with high-order multiple scattering, Physical Review Letters 75 (1995) 4206–4209 (Dec 1995). doi:10.1103/PhysRevLett.75.4206.
URL https://link.aps.org/doi/10.1103/PhysRevLett.75.4206

[24] A. Dubois, K. Belkebir, M. Saillard, Localization and characterization of two-dimensional targets buried in a cluttered environment, Inverse Problems 20 (6) (2004) S63–S79 (nov 2004). doi:10.1088/0266-5611/20/6/s05.

[25] M. A. Haider, K. J. Mehta, J.-P. Fouque, Time-reversal simulations for detection in randomly layered media, Waves in Random Media 14 (2) (2004) 185–198 (2004). arXiv:https://doi.org/10.1088/0959-7174/14/2/007, doi:10.1088/0959-7174/14/2/007.
URL https://doi.org/10.1088/0959-7174/14/2/007

[26] D. Liu, J. Krolik, L. Carin, Electromagnetic target detection in uncertain media: Time-reversal and minimum-variance algorithms, IEEE Transactions on Geoscience and Remote Sensing 45 (4) (2007) 934–944 (April 2007). doi:10.1109/TGRS.2006.890411.

[27] D. Alfaro Vigoa, J.-P. Fouque, J. Garnier, A. Nachbin, Robustness of time reversal for waves in time-dependent random media, Stochastic Processes and their Applications 113 (2) (2004) 289–313 (2004). doi:https://doi.org/10.1016/j.spa.2004.04.002.
URL http://www.sciencedirect.com/science/article/pii/S0304414904000717

[28] G. Bal, R. Verástegui, Time reversal in changing environments, Multiscale Modeling & Simulation 2 (4) (2004) 639–661 (2004). arXiv:https://doi.org/10.1137/030600837, doi:10.1137/030600837.
URL https://doi.org/10.1137/030600837

[29] L. Borcea, G. Papanicolaou, C. Tsogka, Imaging and time reversal in random media, Inverse Problems 18 (5) (2002) 1247–1279 (jul 2002). doi:10.1088/0266-5611/18/5/303.

[30] A. Devaney, Time reversal imaging of obscured targets from multistatic data, IEEE Transactions on Antennas and Propagation 53 (5) (2005) 1600–1610 (2005). doi:10.1109/TAP.2005.846723.
URL http://ieeexplore.ieee.org/lpdocs/epic03/wrapper.htm?arnumber=1427917

[31] B. Samet, S. Amstutz, M. Masmoudi, The Topological Asymptotic for the Helmholtz Equation, SIAM Journal on Control and Optimization 42 (5) (2003) 1523–1544 (2003). doi:10.1137/S0363012902406801.
URL http://epubs.siam.org/doi/abs/10.1137/S0363012902406801

[32] M. Bonnet, B. B. Guzina, Sounding of finite solid bodies by way of topological derivative, International Journal for Numerical Methods in Engineering 61 (December 2003) (2004) 2344–2373 (2004). doi:10.1002/nme.1153.

[33] J. Virieux, S. Operto, An overview of full-waveform inversion in exploration geophysics, Geophysics 74 (6) (2009) WCC1 (2009). doi:10.1190/1.3238367.

[34] B. B. Guzina, M. Bonnet, Topological derivative for the inverse scattering of elastic waves, Q. Jl Mech. Appl. Math. 57 (2) (2004) 161–179 (2004).

[35] A. V. Goncharsky, S. Y. Romanov, S. Y. Seryozhnikov, Inverse problems of 3D ultrasonic tomography with complete and incomplete range data, Wave Motion 51 (3) (2014) 389–404 (2014). doi:10.1016/j.wavemoti.2013.10.001.
URL http://dx.doi.org/10.1016/j.wavemoti.2013.10.001

[36] N. Dominguez, V. Gibiat, Y. Esquerre, Time domain topological gradient and time reversal analogy: an inverse method for ultrasonic target detection, Wave Motion 42 (1) (2005) 31–52 (2005). doi:10.1016/j.wavemoti.2004.09.005.
URL http://www.sciencedirect.com/science/article/pii/S016521250400126X%5Cnhttp://www.sciencedirect.com/scien

[37] S. Rodriguez, M. Deschamps, M. Castaings, E. Ducasse, Guided wave topological imaging of isotropic plates, Ultrasonics 54 (7) (2014) 1880–1890 (2014). doi:10.1016/j.ultras.2013.10.001.
URL http://dx.doi.org/10.1016/j.ultras.2013.10.001

[38] S. Rodriguez, M. Veidt, M. Castaings, E. Ducasse, M. Deschamps, One channel defect imaging in a reverberating medium, Applied Physics Letters 105 (24) (2014) 244107 (dec 2014). doi:10.1063/1.4904837.
URL http://scitation.aip.org/content/aip/journal/apl/105/24/10.1063/1.4904837

[39] R. Tokmashev, A. Tixier, B. B. Guzina, Experimental validation of the topological sensitivity approach to elastic-wave imaging, Inverse Problems 29 (2013) 125005 (2013). doi:10.1088/0266-5611/29/12/125005.

[40] E. Lubeigt, S. Mensah, S. Rakotonarivo, J.-F. Chaix, F. Baqué, G. Gobillot, Topological imaging in bounded elastic media, Ultrasonics 76 (2017) 145–153 (2017). doi:10.1016/j.ultras.2017.01.002.
URL http://linkinghub.elsevier.com/retrieve/pii/S0041624X17300069

[41] S. Rodriguez, M. Castaings, M. Deschamps, E. Ducasse, Topological Imaging of Defects in Anisotropic Plates, in: EWSHM - 7th European Workshop on Structural Health Monitoring, 2014, pp. 1155–1162 (2014).

[42] K. Metwally, E. Lubeigt, S. Rakotonarivo, J.-F. Chaix, F. Baqué, G. Gobillot, S. Mensah, Weld inspection by focused adjoint method, Ultrasonics 83 (2018) 80 – 87 (2018). doi:https://doi.org/10.1016/j.ultras.2017.08.009.
URL http://www.sciencedirect.com/science/article/pii/S0041624X17302706

[43] C. Bellis, M. Bonnet, Qualitative identification of cracks using 3D transient elastodynamic topological derivative: formulation and FE implementation, Computer Methods in Applied Mechanics and Engineering 253 (2013) 89–

105 (2013). doi:10.1016/j.cma.2012.10.006.
URL https://hal.archives-ouvertes.fr/hal-00741515

[44] G. Renaud, P. Kruizinga, D. Cassereau, P. Laugier, In vivo ultrasound imaging of the bone cortex, Physics in medicine and biology 63 (12) (2018) 125010 (June 2018). doi:10.1088/1361-6560/aac784.
URL https://doi.org/10.1088/1361-6560/aac784

[45] W. Ke, M. Castaings, C. Bacon, 3D finite element simulations of an air-coupled ultrasonic NDT system, NDT and E International 42 (6) (2009) 524–533 (2009). doi:10.1016/j.ndteint.2009.03.002.

[46] J.-B. Ihn, F.-K. Chang, Pitch-catch Active Sensing Methods in Structural Health Monitoring for Aircraft Structures, Structural Health Monitoring: An International Journal 7 (1) (2008) 5–19 (2008). doi:10.1177/1475921707081979.
URL http://journals.sagepub.com/doi/10.1177/1475921707081979